

# Efficient visible and UV generation by frequency conversion of a mode-filtered fiber amplifier

Dahv A.V. Kliner<sup>\*a</sup>, Fabio Di Teodoro<sup>b</sup>, Jeffrey P. Koplow<sup>b</sup>, Sean W. Moore<sup>b</sup>, and Arlee V. Smith<sup>c</sup>

<sup>a</sup>Sandia National Laboratories, P.O. Box 969, MS 9056, Livermore, CA 94551

<sup>b</sup>Naval Research Laboratory, Optical Sciences Division, Washington, DC 20375

<sup>c</sup>Sandia National Laboratories, Albuquerque, NM 87185

## ABSTRACT

We have generated the second, third, fourth, and fifth harmonics of the output of a Yb-doped fiber amplifier seeded by a passively Q-switched Nd:YAG microchip laser. The fiber amplifier employed multimode fiber (25  $\mu\text{m}$  core diameter,  $V \approx 7.4$ ) to provide high-peak-power pulses, but diffraction-limited beam quality was obtained by use of bend-loss-induced mode filtering. The amplifier output had a pulse duration of 0.97 ns and smooth, transform-limited temporal and spectral profiles ( $\sim 500$  MHz linewidth). We obtained high nonlinear conversion efficiencies using a simple optical arrangement and critically phase-matched crystals. Starting with 320 mW of average power at 1064 nm (86  $\mu\text{J}$  per pulse at a 3.7 kHz repetition rate), we generated 160 mW at 532 nm, 38 mW at 355 nm, 69 mW at 266 nm, and 18 mW at 213 nm. The experimental results are in excellent agreement with calculations. Significantly higher visible and UV powers will be possible by operating the fiber amplifier at higher repetition rates and pulse energies and by further optimizing the nonlinear conversion scheme.

**Keywords:** Ultraviolet generation, Optical fiber amplifiers, Frequency conversion, Ytterbium

## 1. INTRODUCTION

Compact and efficient sources of visible and ultraviolet (UV) radiation are required for a wide range of applications. In many cases, continuous tunability, broad wavelength coverage, narrow linewidth, high peak or average power, and high beam quality are also needed. Frequency conversion of pulsed, rare-earth-doped fiber lasers and amplifiers offers the possibility of a practical source that simultaneously meets all of these requirements.<sup>1-7</sup> Fiber-based systems have not been widely used for visible and UV generation, however, because of their relatively low pulse energies and peak powers (in comparison to bulk lasers) and consequent low nonlinear conversion efficiency. In the past several years, techniques have been developed for significantly increasing the pulse energy and peak power of fiber sources,<sup>8-13</sup> opening up the possibility of efficient nonlinear frequency conversion throughout the visible and UV spectral regions using standard nonlinear crystals. In this paper, we report generation of the second, third, fourth, and fifth harmonics of a high-pulse-energy, Yb-doped, double-clad (DC) fiber amplifier seeded by a pulsed Nd:YAG microchip laser.<sup>7,13</sup>

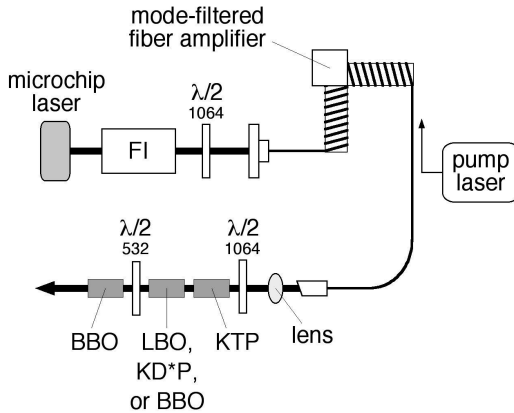
## 2. METHODOLOGY

Figure 1 shows a schematic diagram of the apparatus. In this system, large pulse energies and peak powers were enabled by the use of multimode gain fiber, but diffraction-limited beam quality was obtained by coiling of the fiber to suppress propagation of transverse modes other than the fundamental mode ( $\text{LP}_{01}$ ).<sup>14</sup> Specifically, the Yb-doped fiber

---

\* dakline@ca.sandia.gov; phone (925)294-2821; fax (925)294-2595

had a core diameter and numerical aperture of 25  $\mu\text{m}$  and  $\sim 0.10$ , respectively, which corresponds to a V-number of  $\sim 7.4$  and a measured  $\text{LP}_{01}$  mode-field diameter of 19.5  $\mu\text{m}$  at 1064 nm.<sup>14</sup> For bend-loss-induced mode filtering, the fiber was coiled on two orthogonal spools of 1.67 cm diameter. The DC fiber was pumped near one end using the 976 nm cw output of a formatted diode bar (Limo), which provided up to 17 W of launched pump power (although  $< 3$  W was used for the present experiment). We used the technique of embedded-mirror side pumping, in which a mirror is embedded in a channel polished into the inner cladding of the DC fiber, and pump light is launched by reflection from the mirror.<sup>15</sup>



**Figure 1.** Schematic diagram of the experimental apparatus. FI = Faraday isolator,  $\lambda/2$  = half-wave plate (at the indicated wavelength in nm). Bold lines indicate free-space beams.

The fiber amplifier was seeded with the 1064 nm output of a passively Q-switched Nd:YAG microchip laser (Poly-Scientific). The seed laser produced transform-limited pulses with a nearly Gaussian temporal profile (0.97 ns FWHM) and an energy of  $\sim 10$   $\mu\text{J}$  at a repetition rate of 3.5–3.9 kHz. The seed laser was optically isolated from the amplifier and was coupled into a single-mode fiber, which was fusion spliced to the Yb-doped fiber. The seed and pump beams were counter-propagating. The output end of the DC fiber was mode-stripped to remove light propagating in the inner cladding (similarly, the seed end of the amplifier was mode-stripped by the single-mode pigtail). The input and output facets were fusion spliced to fused-silica beam expanders to prevent optical damage, and both ends were angle-polished at  $8^\circ$  to eliminate feedback. The amplifier produced diffraction-limited output pulses with a temporal profile identical to that of the seed laser.<sup>13</sup> Half-wave plates were used to adjust the polarization of the seed beam and the amplifier output in order to provide linearly polarized light of the correct orientation for the nonlinear crystals.

The amplifier output beam was imaged using an  $f = 11$  mm aspheric lens (Geltech) to a measured beam waist of  $\sim 360$   $\mu\text{m}$  ( $1/e^2$  diameter). The nonlinear crystals were positioned near the beam waist and were angle tuned to maximize the conversion efficiency. In order to provide a compact, rugged, and simple setup, no lenses or other optics were placed between the crystals (other than a wave plate for generation of the fifth harmonic; see below). After passing through the crystal(s), the various harmonics were separated using a fused-silica Pellin-Broca prism, and the pulse energies were measured using either a pyroelectric detector (Moletron) or a biased, silicon photodiode (calibrated against the pyroelectric detector).

The second harmonic (532 nm) of the amplifier output was generated using Type II phase matching in a hydrothermally grown, 9-mm-long KTP crystal (XY cut,  $\theta = 90^\circ$ ,  $\phi = 26^\circ$ ; Poly-Scientific). The fourth harmonic (266 nm) was generated by Type I doubling of the 532 nm light in either a BBO crystal (15 mm,  $48^\circ$ ; Castech) or a KD\*P crystal (20 mm,  $88^\circ$ ; Cleveland Crystals). Alternatively, the third harmonic (355 nm) was generated by Type I mixing of the 532 nm radiation with the residual 1064 nm radiation of the same polarization using LBO (10 mm, XY,  $\theta = 90^\circ$ ,  $\phi = 37^\circ$ ; Castech). Finally, the fifth harmonic (213 nm) was generated by mixing the 532 nm and 355 nm radiation using Type I mixing in BBO (20 mm,  $70^\circ$ ; Castech); a zero-order wave plate (full-wave at 355 nm, half-wave at 532 nm) was inserted between the LBO and BBO crystals to rotate the polarization of the 532 nm beam to be parallel to that of the 355 nm beam. All crystals and wave plates were anti-reflection coated for the appropriate wavelengths on the input and output faces (reflection losses of  $< 0.2\%$  per face).

### 3. RESULTS AND DISCUSSION

The results are summarized in Fig. 2, which shows the pulse energies ( $P_i$ , where  $i$  is the wavelength in nm) and corresponding average powers of the amplifier output and of the various harmonics as a function of current supplied to the pump diode. The measurements (shown as symbols) have been corrected for Fresnel losses on the Pellin-Broca prism (1%–21%, depending on the wavelength and polarization state). At the highest current of 13.3 A, the pulse energies (average powers) were 86  $\mu\text{J}$  (320 mW) at 1064 nm, 43  $\mu\text{J}$  (160 mW) at 532 nm, 10  $\mu\text{J}$  (38 mW) at 355 nm, 19  $\mu\text{J}$  (69 mW) at 266 nm, and 4.7  $\mu\text{J}$  (18 mW) at 213 nm.

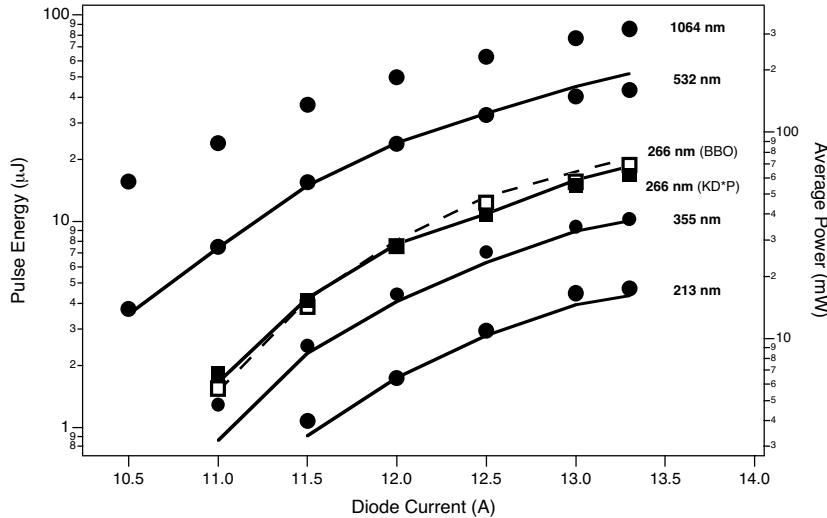


**Figure 2.** Pulse energy (left axis) and corresponding average power (right axis) as a function of current supplied to the pump diode for the amplifier output (1064 nm) and for the indicated harmonics. The points are the experimental results, and the curves are the results of the SNLO calculations for a 420  $\mu\text{m}$  beam diameter at 1064 nm (which gave best agreement for  $P_{532}$  and  $P_{266}$ ; see text).

For peak powers above  $\sim 60$  kW ( $P_{1064}$  above  $\sim 60$   $\mu\text{J}$ ), we observed polarization instability of the amplifier output caused by nonlinear birefringence,<sup>16,17</sup> which resulted in a corresponding instability in the doubling efficiency. The threshold power for the onset of nonlinear birefringence corresponds to a polarization beat length of  $\sim 25$  cm,<sup>16</sup> a reasonable value for commercial fiber.<sup>18</sup> This effect would be eliminated by the use of polarization-maintaining DC fiber,<sup>19</sup> allowing even higher peak powers (as in previous experiments<sup>13</sup>) and conversion efficiencies to be obtained.

We have performed calculations using the SNLO computer program<sup>20</sup> to compare with the experimental results. This analysis took into account the spatial and temporal profiles of the beams, beam divergence (diffraction) and overlap, walk-off in each crystal, and losses between and within the crystals.<sup>7</sup> The calculated results, shown as curves in Fig. 2, are in very good agreement with the measurements.

Figure 3a shows a more detailed comparison of the measurements and calculations for the first stage of frequency doubling. The dashed curve indicates the results of the calculation performed with no adjustable parameters (i.e., with the experimentally determined 1064 nm pulse energy, pulse duration, and beam waist); this calculation slightly overpredicts  $P_{532}$ . The solid curve shows the results of the calculation with the beam diameter increased by 15% (from 360  $\mu\text{m}$  to 420  $\mu\text{m}$ , i.e., within the uncertainty of the beam-waist measurement), which gives nearly perfect agreement with the experiment (the calculations shown in Fig. 2 also correspond to a 420  $\mu\text{m}$  beam diameter). The deviation of the measurements from the calculation for  $P_{1064} > 60$   $\mu\text{J}$  was caused by the nonlinear polarization rotation discussed above. The maximum measured doubling efficiency was 52% (at  $P_{1064} = 63$  and 77  $\mu\text{J}$ ).

The highest value of  $P_{1064}$  corresponds to a peak fluence at the KTP crystal of 160  $\text{MW}/\text{cm}^2$ . For peak fluences above  $\sim 200$   $\text{MW}/\text{cm}^2$ , we observed distortions of the 532 nm beam caused by photorefractive effects in the KTP crystal. The photorefractive threshold could be increased by maintaining the crystal at an elevated temperature,<sup>21</sup> which would permit a smaller beam waist and thus a higher doubling efficiency.

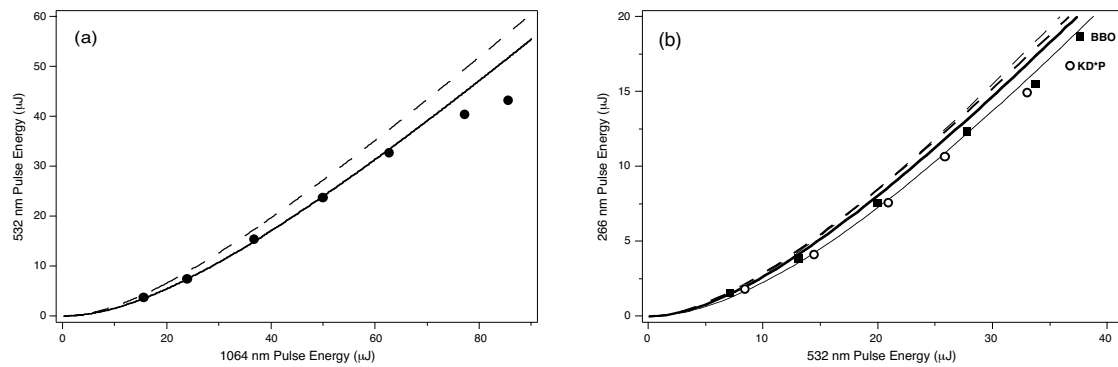


**Figure 3.** (a) Generated 532 nm pulse energy *versus* 1064 nm pulse energy incident on the KTP crystal. The points are the experimental measurements; the curves are the results of the SNLO calculations, with the dashed (solid) curve corresponding to a 360 μm (420 μm) beam diameter. (b) Similar to (a), but showing the 266 nm pulse energy *versus* 532 nm pulse energy. The squares and bold curves correspond to BBO, and the circles and thin curves correspond to KD\*P.

Figure 3b shows the measured and calculated  $P_{266}$  values as a function of  $P_{532}$  incident on the crystal for both BBO and KD\*P. As in Fig. 3a, the calculated  $P_{266}$  values are slightly higher than the measurements, but expanding the beam waist used in the calculation by 15% brings the experimental and theoretical results into nearly perfect agreement. Note that both the experiment and the calculations show almost identical nonlinear conversion efficiencies for the BBO and KD\*P crystals; the 266 nm beam quality is significantly higher when using KD\*P, however, because the walk-off angle in BBO (85 mrad) is much larger than that in KD\*P (2.6 mrad). The maximum doubling efficiency was 50% for BBO and 46% for KD\*P.

The calculated values of  $P_{355}$  and  $P_{213}$  are not strongly dependent on the 1064 nm beam diameter between 360 and 420 μm, and results for a 420 μm diameter are shown in Fig. 2.

Walk-off in the LBO crystal resulted in non-optimal spatial overlap of the 532 and 355 nm beams in the BBO crystal used to generate the fifth harmonic. Figure 4 shows the calculated and measured spatial profiles of the 532 and 355 nm beams at the output face of the LBO crystal. The displacement between beams was calculated using SNLO to be ~110 μm, i.e., ~70% of the calculated 355 nm FWHM beam diameter; the displacement measured using a CCD camera was 69% of the 355 nm FWHM beam diameter, in close accord with the calculation. This displacement could be corrected using a dispersive optical element or dichroic mirrors, which would increase  $P_{213}$  by a factor of >2 according to SNLO calculations.<sup>7</sup>

The seed laser and amplifier produced pulses with a transform-limited linewidth (~0.5 GHz). Although we did not measure the linewidths of the various harmonics, these pulses are also expected to be transform-limited because the acceptance bandwidths of the nonlinear crystals were 40–900 GHz, and dispersion was negligible.

For the present experiment, the amplifier was operated well below its maximum power. At the highest current (13.3 A), the 1064 nm pulse energy, peak power, and average power were 86 μJ, 83 kW, and 320 mW, respectively; we have previously obtained 255 μJ, 305 kW, and 2.2 W with this amplifier (at a repetition rate of 8.5 kHz).<sup>13</sup> Nonetheless, the nonlinear conversion efficiencies were very high because of the high peak power and the diffraction-limited beam quality produced by the mode-filtered fiber amplifier. High conversion efficiencies can also be achieved by using noncritically phase-matched (temperature-tuned) or quasi-phase-matched crystals or by housing the crystals in resonant cavities, but these approaches increase the complexity and limit the tuning range of the system. The ability to use ambient-temperature, critically phase-matched crystals, single-pass mixing, and a simple optical setup (one lens) provides a compact, rugged approach to generation of radiation throughout the visible and UV spectral regions. The present results do not represent the maximum visible and UV powers attainable with fiber sources; by operating the laser system at higher repetition rates and pulse energies and by further optimizing the nonlinear conversion scheme, visible and UV powers of >1 W are possible.

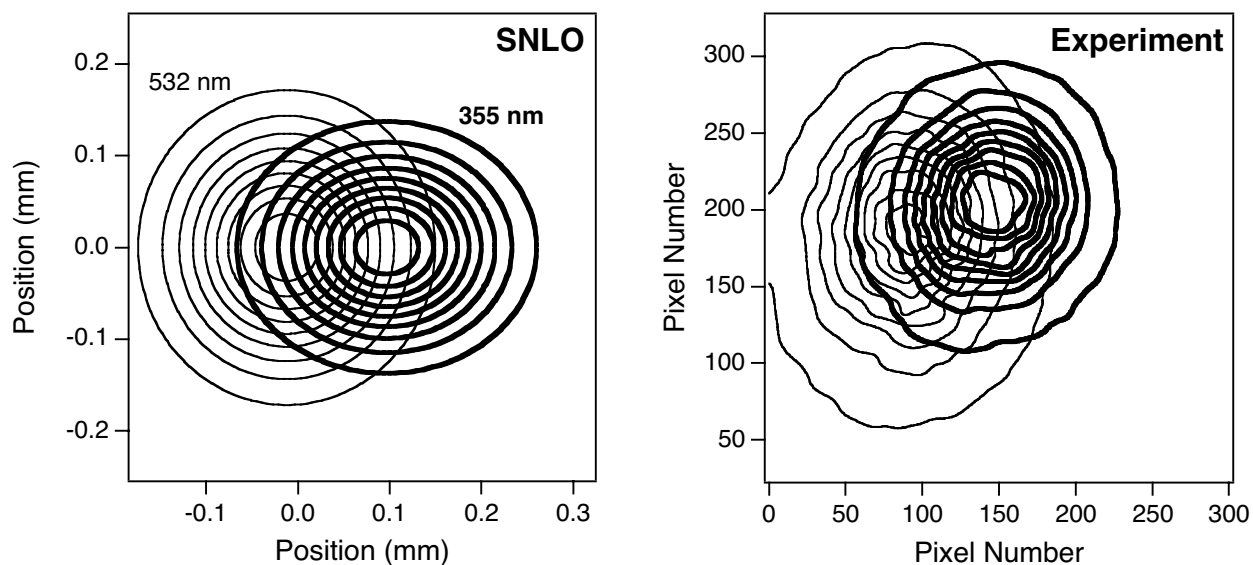


**Figure 4.** Contour plots showing the spatial profiles of the 532 nm (fine lines) and 355 nm (thick lines) beams at the output face of the LBO crystal. The left panel shows the results of the SNLO calculation; the right panel shows the measurement obtained by imaging the output face of the LBO crystal onto a CCD camera using a microscope objective.

#### ACKNOWLEDGMENTS

This work was supported by Sandia's Laboratory Directed Research and Development Program and by the Air Force Philips Laboratory.

#### REFERENCES

1. J.P. Koplow, D.A.V. Kliner, and L. Goldberg, "UV generation by frequency quadrupling of a Yb-doped fiber amplifier", *IEEE Photon. Technol. Lett.* **10**, 75-77 (1998).
2. D. Taverner, P. Briton, P.G.R. Smith, D.J. Richardson, G.W. Ross, and D.C. Hanna, "Highly efficient second-harmonic and sum-frequency generation of nanosecond pulses in a cascaded erbium-doped fiber:periodically poled lithium niobate source", *Opt. Lett.* **23**, 162-164 (1998).
3. S.A. Guskov, S. Popov, S.V. Chernikov, and J.R. Taylor, "Second harmonic generation around 0.53  $\mu\text{m}$  of seeded Yb fibre system in periodically poled lithium niobate", *Electron. Lett.* **34**, 1419-1420 (1998).
4. S.V. Popov, S.V. Chernilov, and J.R. Taylor, "6-W average power green light generation using seeded high power ytterbium fibre amplifier and periodically poled KTP", *Opt. Commun.* **174**, 231-234 (2000)
5. P.A. Champert, S.V. Popov, J.R. Taylor, and J.P. Meyn, "Efficient second-harmonic generation at 384 nm in periodically poled lithium tantalate by use of a visible Yb-Er-seeded fiber source", *Opt. Lett.* **25**, 1252-1254 (2000).
6. G.J. Ray, T.N. Anderson, J.A. Caton, R.P. Lucht, and T. Walther, "OH sensor based on ultraviolet, continuous-wave absorption spectroscopy utilizing a frequency-quadrupled, fiber-amplified external-cavity diode laser", *Opt. Lett.* **26**, 1870-1872 (2001).
7. D.A.V. Kliner, F. Di Teodoro, J.P. Koplow, S.W. Moore, and A.V. Smith, "Efficient second, third, fourth, and fifth harmonic generation of a Yb-doped fiber amplifier", *Opt. Commun.* **210**, 393-398 (2002).

8. D. Taverner, D.J. Richardson, L. Dong, J.E. Caplen, K. Williams, and R.V. Penty, "158- $\mu$ J pulses from a single-transverse-mode, large-mode-area erbium-doped fiber amplifier", *Opt. Lett.* **22**, 378-380 (1997).
9. J. Nilsson, R. Paschotta, J.E. Caplen, and D.C. Hanna, "Yb<sup>3+</sup>-ring-doped fiber for high-energy pulse amplification", *Opt. Lett.* **22**, 1092-1094 (1997).
10. B.C. Dickinson, S.D. Jackson, and T.A. King, "10 mJ total output from a gain-switched Tm-doped fibre laser", *Opt. Commun.* **182**, 199-203 (2000).
11. C.C. Renaud, H.L. Oferhaus, J.A. Alvarez-Chavez, J. Milsson, W.A. Clarkson, P.W. Turner, D.J. Richardson, and A.B. Grudinin, "Characteristics of Q-switched cladding-pumped Ytterbium-doped fiber lasers with different high-energy fiber designs", *IEEE J. Quan. Electron.* **37**, 199-206 (2001).
12. A. Galvanauskas, "Mode-scalable fiber-based chirped pulse amplification systems", *IEEE J. Select. Topics Quan. Electron.* **7**, 504-517 (2001).
13. F. Di Teodoro, J.P. Koplow, S.W. Moore, and D.A.V. Kliner, "Diffraction-limited, 300-kW peak-power pulses from a coiled multimode fiber amplifier", *Opt. Lett.* **27**, 518-520 (2002).
14. J.P. Koplow, D.A.V. Kliner, and L. Goldberg, "Single-mode operation of a coiled multimode fiber amplifier", *Opt. Lett.* **25**, 442-444 (2000).
15. J.P. Koplow, S.W. Moore, and D.A.V. Kliner, "A new method for side pumping of double-clad fiber sources", *IEEE J. Quan. Electron.* (2002, submitted).
16. H.G. Winful, "Polarization instabilities in birefringent nonlinear media: application to fiber-optic devices", *Opt. Lett.* **11**, 33-35 (1986).
17. S.F. Feldman, D.A. Weinberger, and H.G. Winful, "Observation of polarization instabilities and modulational gain in low-birefringence optical fiber", *Opt. Lett.* **15**, 311-313 (1990).
18. S.C. Rashleigh, "Origins and control of polarization effects in single-mode fibers", *IEEE J. Lightwave Technol.* **1**, 312-331 (1983).
19. D.A.V. Kliner, J.P. Koplow, L. Goldberg, A.L.G. Carter, and J.A. Digweed, "Polarization-maintaining amplifier employing double-clad bow-tie fiber", *Opt. Lett.* **26**, 184-186 (2001).
20. A.V. Smith, D.J. Armstrong, and W.J. Alford, "Increased acceptance bandwidths in optical frequency conversion by use of multiple walk-off-compensating nonlinear crystals", *J. Opt. Soc. Am.* **B15**, 122-141 (1998); SNLO can be downloaded at no charge from <http://www.sandia.gov/imrl/XWEB1128/xxtal.htm>.
21. J.K. Tymiński, "Photorefractive damage in KTP used as second-harmonic generator", *J. Appl. Phys.* **70**, 5570-5576 (1991).